

Comprehensive suppression of single-molecule conductance using destructive σ -interference

Marc H. Garner^{1,9}, Haixing Li^{2,6,9}, Yan Chen^{3,9}, Timothy A. Su^{4,7}, Zhichun Shangguan^{3,8}, Daniel W. Paley^{4,5}, Taifeng Liu³, Fay Ng⁴, Hexing Li³, Shengxiong Xiao^{3*}, Colin Nuckolls^{3,4*}, Latha Venkataraman^{2,4*} & Gemma C. Solomon^{1*}

The tunnelling of electrons through molecules (and through any nanoscale insulating and dielectric material¹) shows exponential attenuation with increasing length², a length dependence that is reflected in the ability of the electrons to carry an electrical current. It was recently demonstrated^{3–5} that coherent tunnelling through a molecular junction can also be suppressed by destructive quantum interference⁶, a mechanism that is not length-dependent. For the carbon-based molecules studied previously, cancelling all transmission channels would involve the suppression of contributions to the current from both the π -orbital and σ -orbital systems. Previous reports of destructive interference have demonstrated a decrease in transmission only through the π -channel. Here we report a saturated silicon-based molecule with a functionalized bicyclo[2.2.2]octasilane moiety that exhibits destructive quantum interference in its σ -system. Although molecular silicon typically forms conducting wires⁷, we use a combination of conductance measurements and ab initio calculations to show that destructive σ -interference, achieved here by locking the silicon–silicon bonds into eclipsed conformations within a bicyclic molecular framework, can yield extremely insulating molecules less than a nanometre in length. Our molecules also exhibit an unusually high thermopower (0.97 millivolts per kelvin), which is a further experimental signature of the suppression of all tunnelling paths by destructive interference: calculations indicate that the central bicyclo[2.2.2]octasilane unit is rendered less conductive than the empty space it occupies. The molecular design presented here provides a proof-of-concept for a quantum-interference-based approach to single-molecule insulators.

In molecular electronics, the focus has primarily been on creating devices in which single molecules, bridging the gap between two metal electrodes, mimic the functionality of classical electronic components such as resistors, diodes or switches⁸. Development of highly insulating molecules has been neglected, in part because the coherent electron transport mechanism becomes exponentially more efficient as the dimensions are scaled down. Designing highly insulating sub-nanometre molecules is therefore difficult. A breakthrough at the single-molecule level might hint at a strategy for overcoming the fundamental challenge of direct tunnelling through insulators in classical devices^{9,10}. Here we propose a strategy to create an ideal single-molecule insulator: a molecule bridging a nanometre gap between two metal electrodes across which electronic transmission is completely suppressed. We propose that an ultimate molecular insulator can be achieved using molecules that exhibit complete destructive interference in the transmission.

Figure 1a illustrates the classical example of electronic tunnelling across a vacuum potential barrier^{11,12}. The electronic wavefunction,

which extends into the classical energetically forbidden region between the electrodes, is attenuated; the extent of the attenuation depends exponentially on the separation between the electrodes as shown in Fig. 1b. Inserting a molecule or material between the electrodes will generally result in increased electronic transmission across the gap. Figure 1c illustrates a molecular junction in which transmission is mediated by the frontier molecular orbitals that are coupled to the metal electrodes. As long as the orbitals are not energetically close to the Fermi level of the metal, transmission is in an off-resonant regime, as shown in Fig. 1d. In this regime, if the length of the molecule is increased by adding identical repeat units, such as a methylene group in a linear alkane, transmission decreases exponentially with increasing length (inset, Fig. 1d)². Thus, although alkanes^{8,13} and molecular siloxane¹⁴ have good insulating properties, the transmission across these metal–molecule–metal junctions can always be lowered by removing the molecule. As the junction length decreases, conductance is not effectively suppressed in these insulating systems as the transmission increases exponentially.

Here, we demonstrate a new strategy that relies on a destructive interference effect to suppress coherent transmission across a molecular junction. This effect is a consequence of phase-coherence of the transiting electrons and cannot be modelled by a simple tunnel barrier¹¹. In theory, interference can lead to complete cancellation of the tunnelling probability; consequently, a molecule with complete suppression of the transmission will be less conducting than a vacuum gap of the same dimensions. Destructive interference effects have been demonstrated extensively in recent years, where the focus has been on carbon-based π -conjugated molecules such as a *meta*-linked benzene molecule, as illustrated in Fig. 1e^{4,8}. In such carbon-based wires, transmission can occur through both a π -channel and a σ -channel. Destructive interference annuls transmission completely only in the π -channel and leaves the σ -channel unchanged, as illustrated schematically in Fig. 1f¹³. Thus, the π -conjugated carbon-based systems studied previously cannot achieve complete suppression of the transmission. The lower limit of the conductance will always be set by the conductance of the σ -channel and comparable to an alkane of similar length¹⁵. Additionally, through-space injection from the electrodes into conducting paths can short-circuit the interference effect¹⁶. Therefore, we turn to saturated silicon-based molecules that have solely a σ -orbital system.

In contrast to alkanes, silanes have strong σ -conjugation through their backbones^{17–19}, and linear silane wires are consequently good electrical conductors⁷. It has previously been suggested that destructive quantum interference can be seen in alkanes and silanes in conformations with small dihedral angles in the molecular backbone^{20,21}. We thus designed bicyclo[2.2.2]octasilane, which has *cisoid* Si–Si–Si–Si dihedral angles ranging from 15° to 20° for its three silane bridges. We explore the insulating properties of two methylthiomethyl-functionalized

¹Nano-Science Center and Department of Chemistry, University of Copenhagen, Copenhagen, Denmark. ²Department of Applied Physics and Applied Mathematics, Columbia University, New York, NY, USA. ³The Education Ministry Key Lab of Resource Chemistry, Shanghai Key Laboratory of Rare Earth Functional Materials, Optoelectronic Nano Materials and Devices Institute, Department of Chemistry, Shanghai Normal University, Shanghai, China. ⁴Department of Chemistry, Columbia University, New York, NY, USA. ⁵Columbia Nano Initiative, Columbia University, New York, NY, USA.

⁶Present address: Department of Chemistry, Columbia University, New York, NY, USA. ⁷Present address: Department of Chemistry, University of California, Berkeley, Berkeley, CA, USA. ⁸Present address: School of Chemistry and Chemical Engineering, Shanghai Jiao Tong University, Shanghai, China. ⁹These authors contributed equally: M. H. Garner, H. Li, Y. Chen. *e-mail: xiaosx@shnu.edu.cn; cn37@columbia.edu; lv2117@columbia.edu; gsolomon@chem.ku.dk

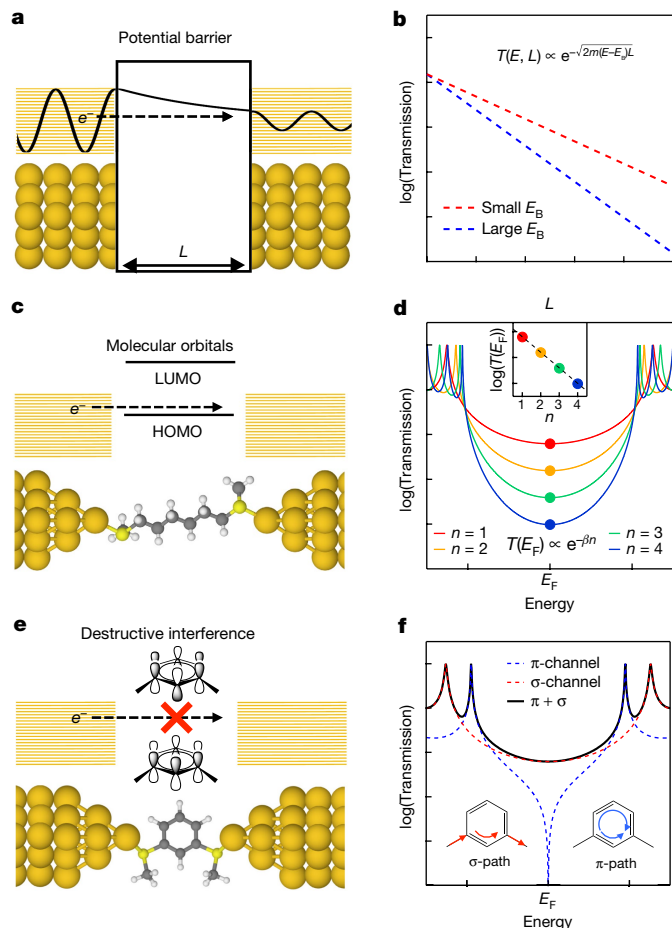


Fig. 1 | Schematic illustration of coherent electron transport and model transmission. **a, b**, Tunnelling through a simple potential energy barrier, E_B , where the transmission probability, $T(E)$, decays exponentially with length, L . **c**, **d**, Schematic of coherent transmission across a molecule. The transmission decays exponentially across a molecular series with n repeat units (inset)². LUMO, lowest unoccupied molecular orbital **e**, **f**, Schematic of coherent transmission across a molecule for which there is destructive quantum interference between contributions from different π -orbitals, as is the case for a meta-coupled benzene unit³². The transmission has contributions from σ - and π -channels; the π -channel is fully suppressed at the antiresonance, but, owing to the σ -contribution, the total transmission does not have an antiresonance¹³.

bicyclo[2.2.2]octasilanes, **Si222** and **Si2-Si222-Si2**, and compare them with the linear silane counterpart **Si4**, which has the same number of silicon atoms as the shortest single path through **Si222** (structures shown in Fig. 2a). Bicyclo[2.2.2]octasilanes have previously been studied theoretically with alternative binding groups, but in that case no appreciable σ -interference was observed²².

We first calculate the Landauer transmission for Au–molecule–Au junctions, using density functional theory (DFT) as detailed in the Methods section, and present the results in Fig. 2b. The transmission at the Fermi energy is two orders of magnitude lower for **Si222** than for its linear counterpart **Si4**, owing to a sharp antiresonance in the transmission close to the Fermi energy. The extended molecule, **Si2-Si222-Si2**, also has an antiresonance close to the Fermi energy, indicating a clear suppression of the transmission by destructive quantum interference. These results are for one of the three conformations of **Si222**; others are shown in Extended Data Fig. 1.

To probe the origin of the interference, we resolve the interatomic transmission pathways²⁰ as illustrated in Fig. 2c–e. The transmission through **Si4** (Fig. 2c) shows one dominant through-bond pathway with no sign of any interference features. The transmissions through **Si222**

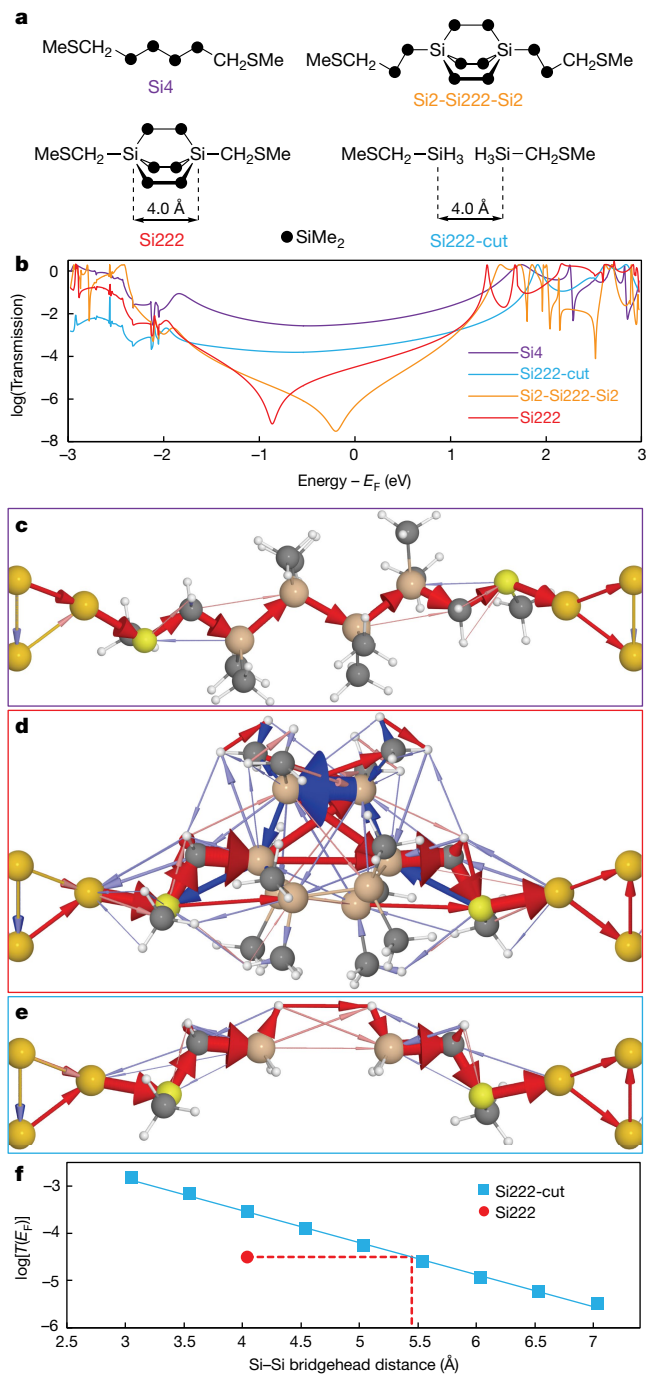


Fig. 2 | Calculated transport properties of Si4, Si222, Si222-cut and Si2-Si222-Si2. **a**, Structures of the molecules investigated. **b**, Landauer transmission plotted semi-logarithmically against energy relative to the Fermi energy. **c–e**, Interatomic transmission pathway analysis of **(c)** **Si4**, **(d)** **Si222** and **(e)** **Si222-cut**. The size of the arrows between atoms is proportional to the magnitude of the transmission contribution, and the colour of the arrows represents the direction (the sign). **Si222** exhibits lower levels of transmission than **Si222-cut** across a wide energy range, indicating that removing the chemical bonds that link the bridgehead silicon atoms increases the transmission. **f**, Transmission at the Fermi energy plotted against bridgehead distance of **Si222** and **Si222-cut**. Solid blue line is a linear fit to the data of **Si222-cut**; dashed red line is a visual guide for comparison.

and **Si2-Si222-Si2** (Fig. 2d and Extended Data Fig. 2c) exhibit ring-current reversal in the bicyclic structure, as indicated by the red and blue arrows, where the sign (colour) reverses in the energy range around the antiresonance (compare with Extended Data Fig. 2c–f).

This is a clear signature of quantum interference; similar features were seen in π -conjugated molecules²⁰. Removing through-bond paths by cutting away the silicon bridges one at a time while passivating the remaining silicon atoms with hydrogens reveals that the interference is gradually lifted as through-bond pathways are disrupted and only the through-space paths remain, as shown in Extended Data Fig. 3. This analysis indicates that the cancellation may occur from destructive interference between the through-space and through-bond paths in **Si222**.

As the origin of interference is in the bicyclic moiety of **Si222**, we compare this unit with the space that it occupies. With all three bridges cut off (**Si222-cut**), the transmission (Fig. 2b) at the Fermi energy is an order of magnitude higher than for **Si222**. That is, the electronic structure of the full molecule is more effective in suppressing transmission than the decay of the wavefunction in the gap between the bridgehead silicon atoms (that is, the terminal atoms of the bicyclic unit) in **Si222-cut**. The pathways of **Si222-cut** (Fig. 2e) show that as the through-bond pathways have been removed, only through-space pathways remain. For comparison, if we perform the same operation with **Si4** and remove a $\text{Si}(\text{CH}_3)_2$ unit, the transmission simply drops as shown in Extended Data Fig. 4. Finally, in Fig. 2f we plot the transmission at the Fermi energy as we manipulate the size of the vacuum gap between the two disjointed silyl groups in **Si222-cut**. This analysis reveals that the transmission in **Si222** corresponds to that of a vacuum gap of just over 5.4\AA , considerably larger than the bridgehead distance of 4.0\AA , and conclusively predicts that destructive interference enables the bicyclic moiety to function as an extremely insulating molecular unit—more insulating than can be achieved by a gap of the same dimensions.

We synthesize **Si4**, **Si222** and **Si2-Si222-Si2** to probe their insulating properties. Briefly, we react dodecamethylbicyclo-[2.2.2]octasilanyl-1,4-dianion²³ with chloromethyl methyl sulfide and 1-chloro(2-methylthiomethyl)tetramethyldisilane to obtain **Si222** and **Si2-Si222-Si2**, respectively, as shown in the scheme in Fig. 3a. **Si4** was synthesized by previously reported methods⁷.

We measure the single Au-molecule-Au junction conductance using a scanning tunnelling microscope break junction (STM-BJ) technique as detailed in the Methods section^{24,25}. In Fig. 3b, we plot logarithmically binned 1D conductance histograms compiled from about 10,000 to 30,000 conductance traces for **Si4**, **Si222** and **Si2-Si222-Si2**, where we observe clear molecular conductance peaks. Two-dimensional conductance-displacement data are shown in Extended Data Fig. 5. In good qualitative agreement with the theoretical predictions presented in Fig. 2, the conductance of **Si222** is an order of magnitude lower than that of **Si4**, and the conductance of **Si2-Si222-Si2** is an order of magnitude lower than that of **Si222**.

We now turn to thermopower measurements²⁶ to probe the slope of the transmission function close to the Fermi energy; if this is large in magnitude, it is highly indicative of an interference effect across the junction^{27,28}. Measurements are carried out as detailed in the Methods section²⁹. For **Si2-Si222-Si2**, we measure a thermopower of about $0.97 \pm 0.03\text{ mV K}^{-1}$ (Fig. 3c), larger than the highest previously reported thermopower of approximately $-33\text{ }\mu\text{V K}^{-1}$ for C_{60} dimer³⁰ and more than 30 times that of its linear silane counterpart **Si8** at about $35 \pm 17\text{ }\mu\text{V K}^{-1}$ (Extended Data Fig. 6). The slope of the calculated transmission is smaller than the experimental values. However, this result is extremely sensitive to the position of the antiresonance relative to the Fermi energy (Extended Data Fig. 6). Given the known errors inherent to DFT calculations and the impact of the experimental environment on the relative alignment of the Fermi level, reliable quantitative agreement between theory and experiment is not achieved for the thermopower^{29,31}. Nevertheless, the large experimental thermopower coefficient presents evidence of a sharp antiresonance in the transmission function near the Fermi level due to destructive quantum interference in this σ -coupled bicyclo[2.2.2]octasilane moiety.

We find, however, that the thermopower for **Si222** is below our measurement resolution, possibly owing to its bulky nature which makes it susceptible to through-space injection directly into

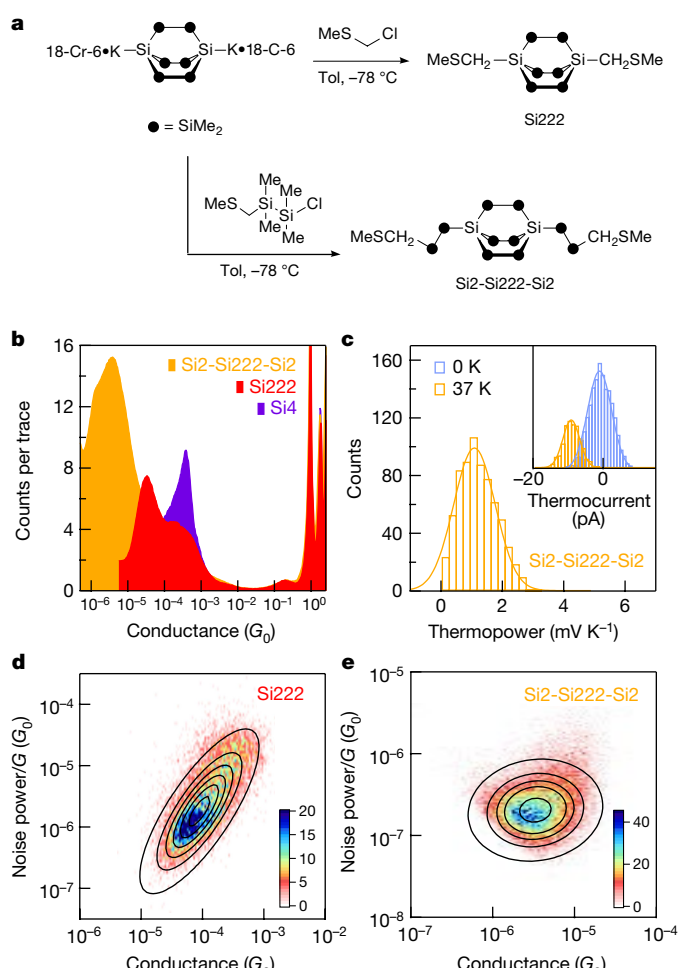


Fig. 3 | Synthesis scheme and experimental single-molecule conductance, thermopower and noise data. **a**, **Si222** and **Si2-Si222-Si2** were synthesized in 40% and 47% yields, respectively, following the scheme shown. Tol, toluene; 18-Cr-6, crown ether 1,4,7,10,13,16-hexaoxacyclooctadecane. **b**, Logarithmically binned 1D conductance histograms for **Si222**, **Si4** and **Si2-Si222-Si2** (100 bins per decade). The bias used for these measurements is: 220 mV for **Si222**, 45 mV for **Si4** and 750 mV for **Si2-Si222-Si2**. The noise floors for the **Si222** and **Si4** histograms have been removed from this figure as they overlap with the peak of **Si2-Si222-Si2**. Note that the conductance for **Si2-Si222-Si2** measured here is an upper bound owing to the large bias used in the measurements. Conductance quantum $G_0 = 2e^2/h$, where e is the charge on an electron, and h is Planck's constant. **c**, Histogram of thermopower determined from the zero-bias thermoelectric current and junction conductance for each **Si2-Si222-Si2** junction measured at a temperature difference of 37 K (approximately 700 junctions). Inset: Histograms of thermoelectric current at temperature differences of 37 K and 0 K between the tip and the substrate. The orange and blue curves are Gaussian fits to the distributions. **d**, **e**, Two-dimensional histograms of normalized flicker noise power plotted against average junction conductance for: (d) **Si222** (10,425 traces) and (e) **Si2-Si222-Si2** (3,000 traces). We determine, from these data, that the noise power scales as G^2 for **Si222** and $G^{0.9}$ for **Si2-Si222-Si2**.

the bicyclic moiety, as detailed in Extended Data Fig. 2a and b. Such a direct injection will result in a smaller slope of the transmission function near the Fermi level, thus yielding a low thermopower with only a modest increase in the conductance. If many of the junctions measured are not fully extended, the thermopower will be low despite the low conductance.

Motivated by the low thermopower of **Si222** but high thermopower in **Si2-Si222-Si2**, we quantify the electron injection path into these molecules through their flicker noise characteristics. Flicker noise

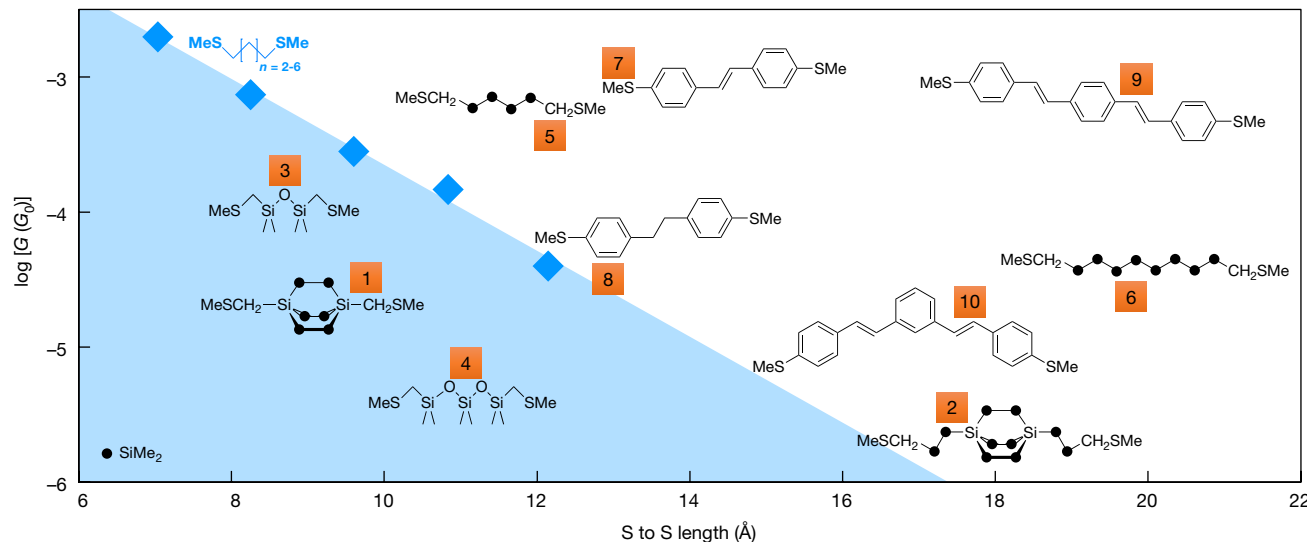


Fig. 4 | Experimental single Au-molecule–Au junction conductance against molecular length. The experimental conductance is plotted semilogarithmically against theoretical direct sulfur-to-sulfur length of the molecules. The blue area denotes molecules that are below the

conductance decay line of alkanes. All conductance values are determined from Au-molecule–Au junctions in published results^{7,14,33} and Extended Data Fig. 8a.

power scales differently with conductance for through-bond and through-space injection from the electrode into the molecule¹⁶. We determine the correlation between the flicker noise power and the respective junction conductance as detailed in the Methods section. By plotting 2D histograms of normalized flicker noise power versus junction conductance G (Fig. 3d and e), we find that the noise power scales as G^2 for **Si222** and as $G^{0.9}$ for **Si2-Si222-Si2**. A scaling of G^2 indicates that conductance is mediated by a through-space coupling, probably from the electrodes directly into the bicyclic structure. The considerable through-space injection in **Si222** is consistent with the high-conductance shoulder seen in the conductance histograms (see Fig. 3b and Extended Data Fig. 5b). By contrast, a scaling of $G^{0.9}$ corresponds to through-bond-dominated transport for the longer **Si2-Si222-Si2** molecule, as the bicyclic moiety is better protected from the electrodes. Control measurements for **Si4** (shown in Extended Data Fig. 5d) show a through-bond conduction as can be expected from the theoretical results in Fig. 2c.

To put the results into the context of highly insulating molecules, we compare the experimental conductance of a range of thiomethyl functionalized molecules with that of **Si222** in Fig. 4. We propose that conductance and length together can provide a measure of the effectiveness of a molecular insulator (analogous to resistivity): thus, we plot the experimental conductance against the calculated sulfur-to-sulfur distance. As alkanes have historically set the standard for insulating molecular moieties, the shaded blue region shows the molecular structures for insulators that are better than alkanes. **Si222** is below the alkane line and even falls just below the strongly insulating siloxane molecular wires¹⁴ (Extended Data Fig. 7a). Those π -conjugated molecules with destructive interference have much lower conductances than those that do not have destructive interference, in agreement with previous studies. However, their experimentally determined conductance (for example, molecule **10**) indicates that they are less insulating than alkanes of the same length. The trends presented in Fig. 4 are independent of binding groups, as measured conductance of amine-terminated molecules display the same trend (Extended Data Fig. 7b).

In recent work, we have shown that linear silanes and siloxanes, to good approximation, mimic the properties of their widely used bulk materials¹⁴. Here we report a different bicyclic molecular form of silicon that is superior to siloxane as a single-molecule insulator. In contrast to previously reported insulating molecules, the mechanism is due to a destructive σ -interference effect within the bicyclic structure

where the Si atoms are constrained to small dihedral angles. Thus, bicyclic silanes represent saturated molecules with clear experimental and calculated signatures of destructive σ -interference. The realization of σ -interference enables the rational design of a new class of highly insulating molecules with extremely low conductance relative to their length, and with very high thermopower.

Online content

Any Methods, including any statements of data availability and Nature Research reporting summaries, along with any additional references and Source Data files, are available in the online version of the paper at <https://doi.org/10.1038/s41586-018-0197-9>.

Received: 14 September 2017; Accepted: 15 March 2018;
Published online 6 June 2018.

- Kingon, A. I., Maria, J.-P. & Streiffer, S. K. Alternative dielectrics to silicon dioxide for memory and logic devices. *Nature* **406**, 1032–1038 (2000).
- Nitzan, A. Electron transmission through molecules and molecular interfaces. *Annu. Rev. Phys. Chem.* **52**, 681–750 (2001).
- Mayor, M. et al. Electric current through a molecular rod—relevance of the position of the anchor groups. *Angew. Chem. Int. Ed.* **42**, 5834–5838 (2003).
- Guédron, C. M. et al. Observation of quantum interference in molecular charge transport. *Nat. Nanotech.* **7**, 305–309 (2012).
- Arroyo, C. R. et al. Signatures of quantum interference effects on charge transport through a single benzene ring. *Angew. Chem. Int. Ed.* **52**, 3152–3155 (2013).
- Sautet, P. & Joachim, C. Electronic interference produced by a benzene embedded in a polyacetylene chain. *Chem. Phys. Lett.* **153**, 511–516 (1988).
- Su, T. A., Li, H., Steigerwald, M. L., Venkataraman, L. & Nuckolls, C. Stereoelectronic switching in single-molecule junctions. *Nat. Chem.* **7**, 215–220 (2015).
- Su, T. A., Neupane, M., Steigerwald, M. L., Venkataraman, L. & Nuckolls, C. Chemical principles of single-molecule electronics. *Nat. Rev. Mater.* **1**, 16002 (2016).
- Ha, Y.-G., Everaerts, K., Hersam, M. C. & Marks, T. J. Hybrid gate dielectric materials for unconventional electronic circuitry. *Acc. Chem. Res.* **47**, 1019–1028 (2014).
- Robertson, J. & Wallace, R. M. High-K materials and metal gates for CMOS applications. *Mater. Sci. Eng. Rep.* **88**, 1–41 (2015).
- Simmons, J. G. Generalized formula for the electric tunnel effect between similar electrodes separated by a thin insulating film. *J. Appl. Phys.* **34**, 1793–1803 (1963).
- Trouwborst, M. L. et al. Transition voltage spectroscopy and the nature of vacuum tunneling. *Nano Lett.* **11**, 614–617 (2011).
- Andrews, D. Q., Solomon, G. C., Van Duyne, R. P. & Ratner, M. A. Single molecule electronics: increasing dynamic range and switching speed using cross-conjugated species. *J. Am. Chem. Soc.* **130**, 17309–17319 (2008).

14. Li, H. et al. Extreme conductance suppression in molecular siloxanes. *J. Am. Chem. Soc.* **139**, 10212–10215 (2017).
15. Borges, A., Fung, E. D., Ng, F., Venkataraman, L. & Solomon, G. C. Probing the conductance of the σ -system of bipyridine using destructive interference. *J. Phys. Chem. Lett.* **7**, 4825–4829 (2016).
16. Adak, O. et al. Flicker noise as a probe of electronic interaction at metal–single molecule interfaces. *Nano Lett.* **15**, 4143–4149 (2015).
17. Tsuji, H., Michl, J. & Tamao, K. Recent experimental and theoretical aspects of the conformational dependence of UV absorption of short chain peralkylated oligosilanes. *J. Organomet. Chem.* **685**, 9–14 (2003).
18. Tsuji, H., Terada, M., Toshimitsu, A. & Tamao, K. $\sigma\sigma^*$ transition in *anti,cisoid* alternating oligosilanes: clear-cut evidence for suppression of conjugation effect by a *cisoid* turn. *J. Am. Chem. Soc.* **125**, 7486–7487 (2003).
19. Bande, A. & Michl, J. Conformational dependence of σ -electron delocalization in linear chains: permethylated oligosilanes. *Chem. Eur. J.* **15**, 8504–8517 (2009).
20. Solomon, G. C., Herrmann, C., Hansen, T., Mujica, V. & Ratner, M. A. Exploring local currents in molecular junctions. *Nat. Chem.* **2**, 223–228 (2010).
21. George, C. B., Ratner, M. A. & Lambert, J. B. Strong conductance variation in conformationally constrained oligosilane tunnel junctions. *J. Phys. Chem. A* **113**, 3876–3880 (2009).
22. Lofas, H., Emanuelsson, R., Ahuja, R., Grigoriev, A. & Ottosson, H. Conductance through carbosilane cage compounds: a computational investigation. *J. Phys. Chem. C* **117**, 21692–21699 (2013).
23. Fischer, R., Konopa, T., Ulliy, S., Baumgartner, J. & Marschner, C. Route Si₆ revisited. *J. Organomet. Chem.* **685**, 79–92 (2003).
24. Xu, B. & Tao, N. J. Measurement of single-molecule resistance by repeated formation of molecular junctions. *Science* **301**, 1221 (2003).
25. Venkataraman, L. et al. Single-molecule circuits with well-defined molecular conductance. *Nano Lett.* **6**, 458–462 (2006).
26. Reddy, P., Jang, S.-Y., Segalman, R. A. & Majumdar, A. Thermoelectricity in molecular junctions. *Science* **315**, 1568 (2007).
27. Paulsson, M. & Datta, S. Thermoelectric effect in molecular electronics. *Phys. Rev. B* **67**, 241403 (2003).
28. Bergfield, J. P., Solis, M. A. & Stafford, C. A. Giant thermoelectric effect from transmission supernodes. *ACS Nano* **4**, 5314–5320 (2010).
29. Widawsky, J. R., Darancet, P., Neaton, J. B. & Venkataraman, L. Simultaneous determination of conductance and thermopower of single molecule junctions. *Nano Lett.* **12**, 354–358 (2012).
30. Rincón-García, L., Evangelisti, C., Rubio-Bollinger, G. & Agrait, N. Thermopower measurements in molecular junctions. *Chem. Soc. Rev.* **45**, 4285–4306 (2016).
31. Tamblyn, I., Darancet, P., Quek, S. Y., Bonev, S. A. & Neaton, J. B. Electronic energy level alignment at metal–molecule interfaces with a GW approach. *Phys. Rev. B* **84**, 201402 (2011).
32. Yoshizawa, K., Tada, T. & Staykov, A. Orbital views of the electron transport in molecular devices. *J. Am. Chem. Soc.* **130**, 9406–9413 (2008).
33. Aradhya, S. V. et al. Dissecting contact mechanics from quantum interference in single-molecule junctions of stilbene derivatives. *Nano Lett.* **12**, 1643–1647 (2012).

Acknowledgements G.C.S. and M.H.G. received funding from the Danish Council for Independent Research | Natural Sciences and the Carlsberg Foundation. We thank the National Science Foundation (NSF) for the support of experimental studies under grant no. CHE-1404922 (Ha.L.) and Columbia University's Research Initiatives in Science and Engineering. Y.C., Z.S., T.L. and S.X. are sponsored by the National Natural Science Foundation of China (grant nos 21473113 and 51502173), the Program for Professor of Special Appointment (Eastern Scholar) at Shanghai Institutions of Higher Learning (no. 2013-57), the "Shuguang Program" supported by Shanghai Education Development Foundation and Shanghai Municipal Education Commission (14SG40), the Program of Shanghai Academic/Technology Research Leader (no. 16XD1402700), the National Natural Science Foundation of Shanghai (no. 15ZR1431100), the Ministry of Education of China (PCSIRT_16R49) and the International Joint Laboratory of Resource Chemistry (IJLRC). T.A.S. was supported by an NSF Graduate Research Fellowship under grant no. 11-44155. We thank B. Fowler for mass spectrometry characterization. Single-crystal X-ray diffraction was performed at the Shared Materials Characterization Laboratory (SMCL) at Columbia University. Use of the SMCL was made possible by funding from Columbia University.

Author contributions M.H.G., Ha.L., T.A.S., C.N., L.V. and G.C.S. conceived the idea for the paper. M.H.G. conducted the theoretical calculations under the supervision of G.C.S. Ha.L. did the conductance, noise and thermopower measurements under the supervision of L.V. Y.C., T.A.S., Z.S., D.W.P. and T.L. synthesized and characterized the molecules under the supervision of F.N., He.L., C.N. and S.X. M.H.G., Ha.L., L.V. and G.C.S. analysed the data and wrote the paper with contributions from all authors.

Competing interests The authors declare no competing financial interests.

Additional information

Extended data is available for this paper at <https://doi.org/10.1038/s41586-018-0197-9>.

Reprints and permissions information is available at <http://www.nature.com/reprints>.

Correspondence and requests for materials should be addressed to G.C.S., L.V., C.N. or S.X.

Publisher's note: Springer Nature remains neutral with regard to jurisdictional claims in published maps and institutional affiliations.

METHODS

Theory. We model the single-molecule junction conductance as coherent tunnelling using the Landauer–Büttiker scattering formalism. The Landauer transmission is calculated using the equilibrium limit of the non-equilibrium Green's functions (NEGF) approach as described in detail elsewhere³⁴. We optimize all molecules in vacuum to a force threshold of 0.01 eV Å⁻¹ for all atoms using DFT with the Perdew–Burke–Ernzerhof correlation–exchange (PBE XC) functional³⁵ and double- ζ plus polarization (DZP) basis set as implemented in the Atomic Simulation Environment (ASE) and GPAW software packages^{36–38}. We use a systematic algorithm for building single-molecule junctions in ASE. We place the tip Au-atoms on the optimized molecules in positions corresponding to a fully extended junction. Based on test optimizations, we use the following parameters: Au–S distance 2.45 Å, Au–S–CH₂ bond angle 110°, Au–S–CH₂–Si dihedral angle ±170°. Based on the position of the tip Au-atoms, we build two four-atom Au pyramids (tetrahedrons) and place these on a 4 × 4 × 4 Au face-centred cubic (fcc) (111) slab to form a single-molecule junction with periodic boundary conditions in all directions. We relax the junction structures to 0.05 eV Å⁻¹ using DFT with the PBE XC functional, DZP basis set for the molecule and double- ζ (DZ) basis set for the Au atoms, two k -points in the irreducible part of the Brillouin zone for the x - and y -directions, and one k -point for the z -direction (the transport direction of the junction). The optimized junction structures (the two Au-pyramids and the molecule) are placed between semi-infinite 6 × 6 Au fcc111 surfaces, and the Landauer transmission is calculated using the NEGF approach as implemented in Atomistix Tool Kit (ATK) software package^{34,39–41}. The transmission is calculated using DFT with the PBE XC functional, DZP basis set for the molecule and DZ basis set for the Au atoms, one k -point in the irreducible part of the Brillouin zone for the x - and y -directions, and 200 k -points for the z -direction (the transport direction of the junction). We resolve the interatomic transmission pathways at the Fermi energy as described in detail elsewhere²⁰. The transmission contributions between atoms are plotted as arrows on top of the optimized junction structures in Fig. 2. At any surface across the junction, the sum of arrows reproduces the full transmission. The cross-sectional area of the arrows scales proportionally with the magnitude of the interatomic transmission. We apply a threshold of 5% of the total transmission for the pathways. Pathways between 5% and 20% of the total transmission are plotted in dimmed colours. Note that when there is destructive quantum interference, the magnitude of one pathway can be larger than the total transmission. We use two Au ghost atoms to provide extra basis functions when calculating the transmission through vacuum for **Si222-cut** as presented in Fig. 2f. Tests show that the extra ghost atom basis functions are only needed for Si–Si gaps over 4.5 Å. Therefore, ghost atoms are not needed for the transmission plotted in Fig. 2b, and consequently we can calculate the transmission pathways as shown in Fig. 2a without ghost atoms. We have tested that the through-space H–Si–Si–H dihedral between the two silyl groups of **Si222-cut** has no noticeable effect on the transmission.

Synthesis. All reactions were performed in oven-dried or flame-dried round-bottom flasks, unless otherwise noted. The flasks were fitted with rubber septa, and reactions were conducted under a positive pressure of nitrogen or argon, unless otherwise noted. THF, hexane and toluene were obtained from a Schlenk manifold with purification columns packed with activated alumina and supported copper catalyst (Glass Contour). Commercial reagents were used without further purification. Dichlorodimethylsilane and dichlorotetramethyldisilane were purchased from TCL. All other reagents were purchased from Sigma-Aldrich. 1,4-bis(trimethylsilyl)dodecamethylbicyclo[2.2.2]octasilane was synthesized according to previously reported methods²³.

1-chloro-2-(methylthiomethyl)tetramethyldisilane **1**: A 500-ml three-neck round-bottom flask was equipped with a stir bar, addition funnel and condenser. Magnesium turnings (14.5 g, 0.6 mol, 2.07 equiv.) were activated with a small crystal of iodine in 10 ml of THF. We subsequently added 190 ml of THF. We added chloromethyl methyl sulfide (0.29 mol, 24.3 ml, 1.00 equiv.) dropwise through the addition funnel over a period of 1 h. During this period, the temperature of the reaction system was kept at 10–20 °C by cooling with an ice–water bath; maintenance of the reaction temperature between 10 and 20 °C is important to the successful generation of the Grignard reagent. After stirring at room temperature for an additional hour, we cannula transferred the solution and passed it through a Schlenk filter to give methylthiomethylmagnesium chloride as an assumed 1.45 M solution in THF, which was subsequently added dropwise to dichlorotetramethyldisilane (0.29 mol, 54.29 g, 1.00 equiv.) in THF (480 ml) at room temperature. The mixture was heated under reflux for 6 h. THF was removed under reduced pressure and hexane was added to the residue. The hexane solution was filtered over Celite through a Schlenk filter into a Schlenk flask. The solvent was removed in vacuo, and the crude compound was vacuum distilled to yield **1** as a light yellow oil (46.30 g, 75%). ¹H NMR (400 MHz, C₆D₆) δ 1.84, 1.69, 0.45, 0.19. ¹³C NMR (101 MHz, C₆D₆) δ 20.39, 19.27, 2.75, –4.50. ²⁹Si NMR (79 MHz, C₆D₆) δ

22.76, –16.50. High-resolution mass spectrometry (HRMS) could not be obtained because of the sensitivity of the compound to water.

Si222: We added 1,4-bis(trimethylsilyl)dodecamethylbicyclo[2.2.2]octasilane²³ (0.557 g, 1.01 mmol, 1 equiv.), *tert*-BuOK (0.226 g, 2.02 mmol, 2 equiv.) and 18-crown-6 (0.534 g, 2.02 mmol, 2 equiv.) to a 100-ml Schlenk flask, followed by toluene (20 ml). The mixture was stirred overnight to generate the octasilyl dianion. This solution was then added dropwise to a solution of chloromethyl methyl sulfide (0.195 g, 2.02 mmol, 2 equiv.) in 40 ml of toluene cooled to –78 °C in a bath of dry ice plus acetone. The reaction mixture was allowed to warm up to room temperature and stirred for 4 h. The reaction mixture was quenched with 2 M H₂SO₄ and extracted three times with diethyl ether. The organic layers were combined, dried over magnesium sulfate and concentrated in vacuo. The crude residue was purified by silica gel chromatography (gradient from hexanes to 7:3 hexanes:dichloromethane) to give a white solid (213 mg, 40%). ¹H NMR (400 MHz, CDCl₃) δ 2.18 (s, 4H), 2.18 (s, 6H), 0.31 (s, 36H). ¹³C NMR (101 MHz, CDCl₃) δ 22.06, 15.00, –2.65. ²⁹Si NMR (79 MHz, CDCl₃) δ –39.30, –75.79; HRMS (fast atom bombardment, FAB+): calculated for C₁₆H₄₆S₂Si₈ 526.12, found [M+H]⁺ 527.13. Single crystals for X-ray diffraction were grown from vapour diffusion of methanol into a concentrated solution of **Si222** in toluene. The mass spectroscopic data were obtained at the Columbia University mass spectrometry facility using a JEOL JMSHX110A/110A tandem mass spectrometer.

Si2-Si222-Si2: 1,4-bis(trimethylsilyl)dodecamethylbicyclo[2.2.2]octasilane²³ (0.557 g, 1.01 mmol, 1 equiv.), *tert*-BuOK (0.226 g, 2.02 mmol, 2 equiv.) and 18-crown-6 (0.534 g, 2.02 mmol, 2 equiv.) were added to a 100 ml Schlenk flask, followed by toluene (20 ml) and the mixture was stirred overnight to generate the octasilyl dianion. This solution was then added dropwise to a solution of **1** (0.430 g, 2.02 mmol, 2 equiv.) in 40 ml of toluene cooled to –78 °C in a dry ice/acetone bath. The reaction mixture was allowed to warm up to room temperature and stirred for 4 h. The reaction mixture was quenched with 2 M H₂SO₄ and extracted three times with diethyl ether. The organic layers were combined, dried over magnesium sulfate and concentrated in vacuo. The crude residue was purified by silica gel chromatography (gradient from hexanes to 7:3 hexanes:dichloromethane) to give a white solid (360 mg, 47%). ¹H NMR (400 MHz, CDCl₃) δ 2.16 (s, 6H), 1.93 (s, 4H), 0.33 (s, 12H), 0.31 (s, 36H), 0.22 (s, 12H). ¹³C NMR (101 MHz, CDCl₃) δ 20.76, 20.59, –0.54, –0.68, –3.22. ²⁹Si NMR (79 MHz, CDCl₃) δ –14.47, –35.06, –37.18, –126.44; HRMS (FAB+): calculated for C₂₄H₇₀S₂Si₁₂ 758.22, found [M+H]⁺ 759.22. Single crystals for X-ray diffraction were grown from vapour diffusion of methanol into a concentrated solution of **Si2-Si222-Si2** in toluene.

Conductance measurements. We measure the single-molecule conductance using the scanning tunnelling microscope break-junction technique with a custom-built set-up described previously²⁵. Briefly, we drive a gold tip in and out of contact with a gold-on-mica substrate and record the conductance (current/voltage) of the junction as the tip is withdrawn. Upon rupture of the Au contact, a molecule may bridge the gap as evidenced by an additional plateau in the trace of conductance versus displacement. We collect 10,000 to 30,000 such traces, which contain 2,000 data points per nanometre of extension (40 kHz sampling rate), and construct the 1D and 2D conductance histograms without data selection. The histograms are normalized by the number of traces used to construct them. All silanes studied here were introduced into the set-up in a 1,2,4-trichlorobenzene solution with 0.1–1 mM concentration.

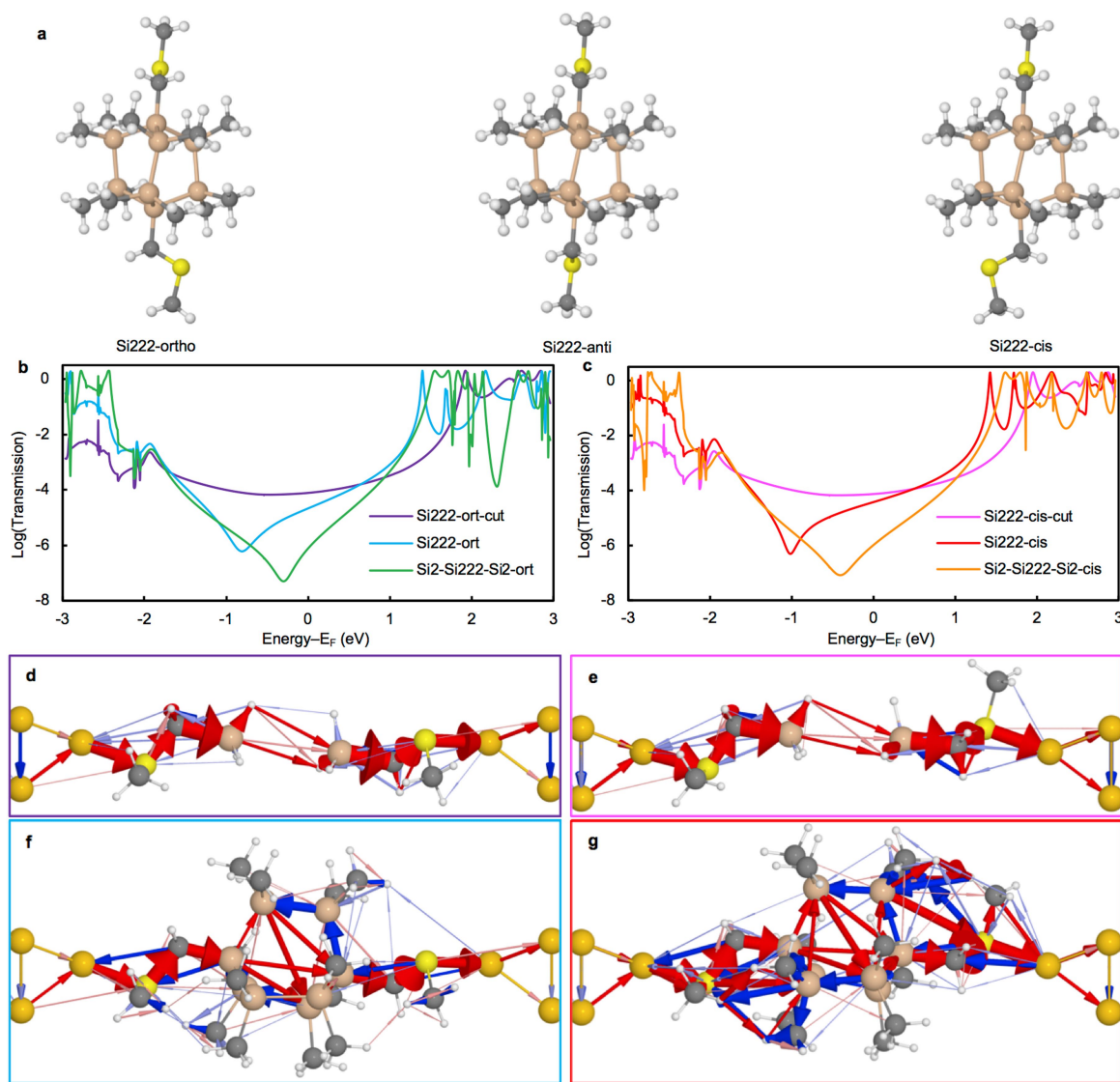
Thermopower measurements. We determined the thermopower of each molecule by performing break-junction measurements with an applied temperature gradient and no applied voltage, as described previously²⁹. Briefly, we heat the substrate and measure the temperature of the substrate and the tip to determine the temperature difference (ΔT) between them. For the work reported here, we have $\Delta T = 0$ K, 27 K and 37 K. We then form a contact between the tip and substrate (at a constant applied voltage) in an environment of the molecules and then break the contact by withdrawing the tip from the substrate at a speed of 20 nm s⁻¹. After a fixed elongation of 2.5 nm, we hold the junction for 5 ms while the bias (750 mV for **Si2-Si222-Si2**, 45 mV for **Si4** and 220 mV for **Si222**) is applied to measure the junction conductance. We then drop the applied bias voltage to zero and hold the junction for an additional 50 ms while measuring the current. The average current during this time is the average thermoelectric current (I). Following this, we turn on the bias again, hold the junction for an additional 5 ms and then pull the junction apart. We determine the conductance (G) just before and after measuring the thermoelectric current. If both conductances are within the molecular histogram peak, as determined from standard conductance measurement, we select the trace. This is done through an automated algorithm. We typically find that 10% of all measured traces (about 5,000–10,000 traces were taken per molecule) have a molecule while the thermoelectric current is measured and are therefore selected. We determine the thermopower as $S = I/(G\Delta T)$ for each junction measured and compile data from hundreds of junctions into the histogram. The Au thermopower of 2 μ V K⁻¹ is subtracted from the reported data.

Flicker noise measurements. We characterized the conductance noise of the molecular junctions to differentiate between through-bond and through-space charge transport using a method described previously¹⁶. To measure the noise, we pause the elongation procedure for 100 ms (as detailed above for the thermoelectric current measurement) and record the conductance at a bias of 220 mV or 750 mV (for **Si222** and **Si2-Si222-Si2**, respectively) with a 100-kHz sampling rate. We select traces that sustain a molecular junction (as detailed above) during the hold period and calculate the discrete Fourier transform of this data. Two quantities are calculated from the measured conductance while the junction is held for each of these traces: the average conductance (G) and the normalized noise power (power spectrum density (PSD)/ G). The PSD is obtained from the square of the integral of the discrete Fourier transform of the measured conductance between 100 Hz to 1000 Hz. The lower frequency limit is constrained by the mechanical stability of the set-up. The upper limit is determined by the input noise of the current amplifier. Using these quantities, we create 2D histograms of the normalized noise power against the average conductance. The relation between noise power and conductance is extracted by determining the exponent n for which PSD/ G and G are not correlated. We have previously shown that the relationship between flicker noise power and junction conductance follows a power law dependence (PSD proportional to G^n) with the scaling exponent (n) being indicative of the electronic coupling type: $n = 1$ is characteristic of through-bond coupling whereas $n = 2$ is characteristic for through-space coupled junctions. Details of these derivations are presented elsewhere¹⁶.

Data availability. The data that support the findings of this study are available from the corresponding authors upon reasonable request. Crystallographic data for the structures reported in this paper have been deposited at the Cambridge Crystallographic Data Centre (CCDC) under the deposition numbers CCDC 1571457 (**Si222**) and CCDC 1571458 (**Si2-Si222-Si2**). Copies of the data can be obtained free of charge from www.ccdc.cam.ac.uk/data_request/cif.

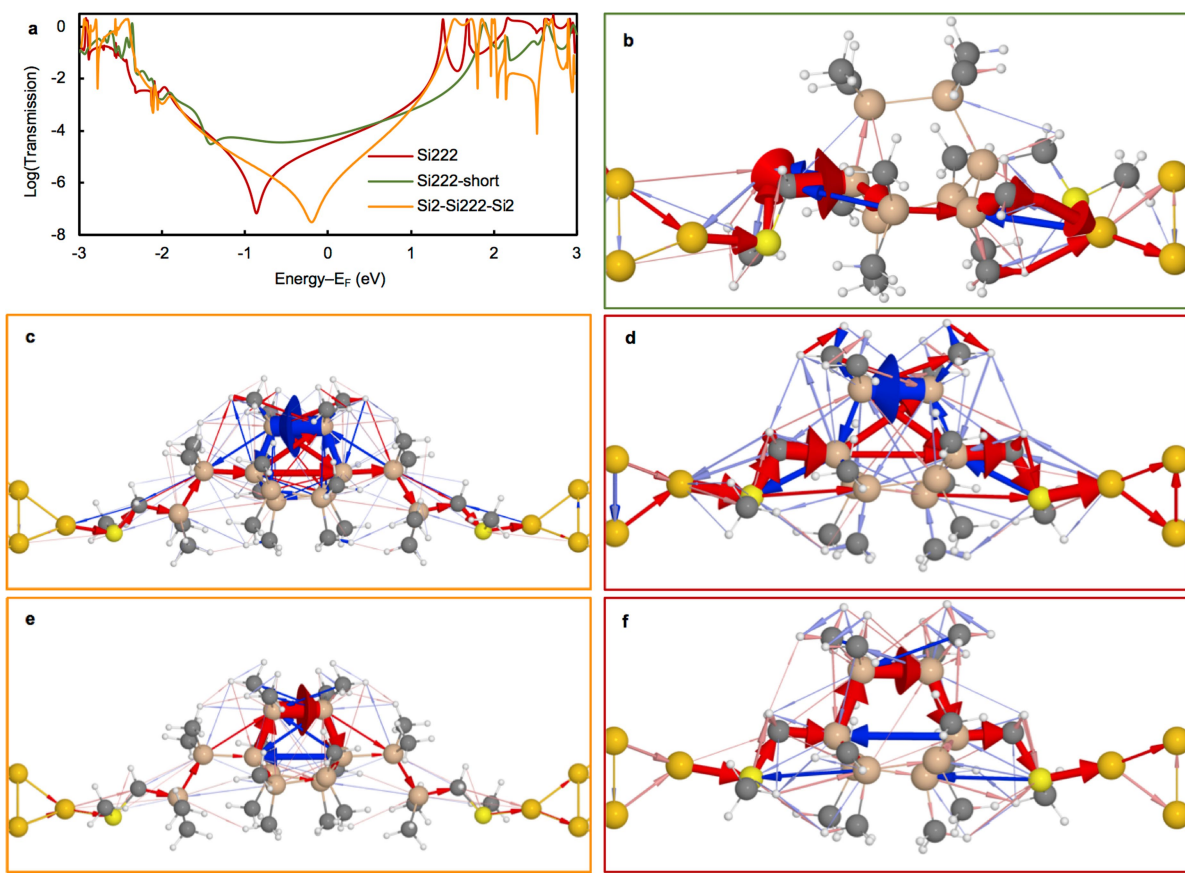
Code availability. The data that support the experimental findings were acquired using a custom instrument controlled by custom software (Igor Pro, Wavemetrics). The software is available from the corresponding author upon reasonable request.

34. Brandbyge, M., Mozos, J.-L., Ordejón, P., Taylor, J. & Stokbro, K. Density-functional method for nonequilibrium electron transport. *Phys. Rev. B* **65**, 165401 (2002).
35. Perdew, J. P., Burke, K. & Ernzerhof, M. Generalized gradient approximation made simple. *Phys. Rev. Lett.* **77**, 3865–3868 (1996).
36. Bahn, S. R. & Jacobsen, K. W. An object-oriented scripting interface to a legacy electronic structure code. *Comput. Sci. Eng.* **4**, 56–66 (2002).
37. Mortensen, J. J., Hansen, L. B. & Jacobsen, K. W. Real-space grid implementation of the projector augmented wave method. *Phys. Rev. B* **71**, 035109 (2005).
38. Larsen, A. H., Vanin, M., Mortensen, J. J., Thygesen, K. S. & Jacobsen, K. W. Localized atomic basis set in the projector augmented wave method. *Phys. Rev. B* **80**, 195112 (2009).
39. Soler, J. M. et al. The SIESTA method for ab initio order- N materials simulation. *J. Phys. Condens. Matter* **14**, 2745 (2002).
40. Atomistix ToolKit version 2016.3 (QuantumWise A/S, 2016); www.quantumwise.com.
41. Virtual NanoLab version 2016.3 (QuantumWise A/S, 2016); www.quantumwise.com.
42. Markussen, T., Jin, C. & Thygesen, K. S. Quantitatively accurate calculations of conductance and thermopower of molecular junctions. *Phys. Status Solidi B* **250**, 2394–2402 (2013).
43. Venkataraman, L., Klare, J. E., Nuckolls, C., Hybertsen, M. S. & Steigerwald, M. L. Dependence of single-molecule junction conductance on molecular conformation. *Nature* **442**, 904–907 (2006).
44. Su, T. A., Li, H., Steigerwald, M. L., Venkataraman, L. & Nuckolls, C. Stereoelectronic switching in single-molecule junctions. *Nat. Chem.* **7**, 215–220 (2015).
45. Park, Y. S. et al. Contact chemistry and single-molecule conductance: a comparison of phosphines, methyl sulfides, and amines. *J. Am. Chem. Soc.* **129**, 15768–15769 (2007).
46. Kim, T., Vázquez, H., Hybertsen, M. S. & Venkataraman, L. Conductance of molecular junctions formed with silver electrodes. *Nano Lett.* **13**, 3358–3364 (2013).
47. Meissner, J. S. et al. Importance of direct metal– π coupling in electronic transport through conjugated single-molecule junctions. *J. Am. Chem. Soc.* **134**, 20440–20445 (2012).
48. Li, H. et al. Silver makes better electrical contacts to thiol-terminated silanes than gold. *Angew. Chem. Int. Ed.* **56**, 14145–14148 (2017).



Extended Data Fig. 1 | The three conformations of Si222 and Si2-Si222-Si2, and their transmission data. **a**, Optimized structures of the three conformations of Si222. **b, c**, Calculated Landauer transmission

for the *ortho* (**b**) and *cis* (**c**) conformations, which are very similar to that of the anti-conformation shown in Fig. 2. **d–g**, Transmission pathways for: (**d**) Si222-*ortho*-cut, (**e**) Si222-*cis*-cut, (**f**) Si222-*ortho* and (**g**) Si222-*cis*.

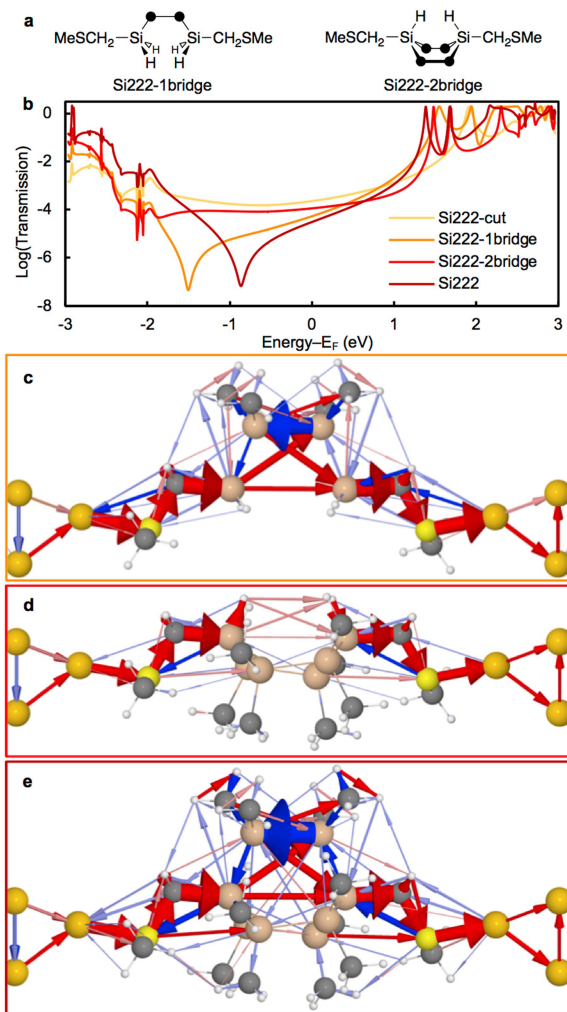


Extended Data Fig. 2 | Transmission data for Si222, Si222-short (a compressed junction of Si222) and Si2-Si222-Si2 anti-conformations.

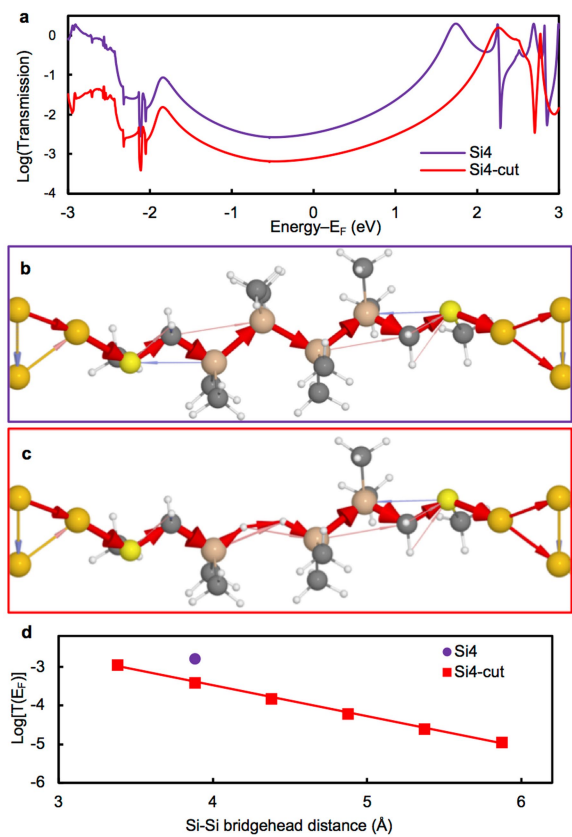
a, Transmission plot; b–d, transmission pathways of (b) Si222-short, (c) Si2-Si222-Si2 and (d) Si222 calculated at 0 eV (the Fermi energy); e, Si2-Si222-Si2 calculated at -0.6 eV; f, Si222 calculated at -1.6 eV.

Through-space injection dominates on one side of the molecule in Si222-short at 0 eV and a flattened transmission function around

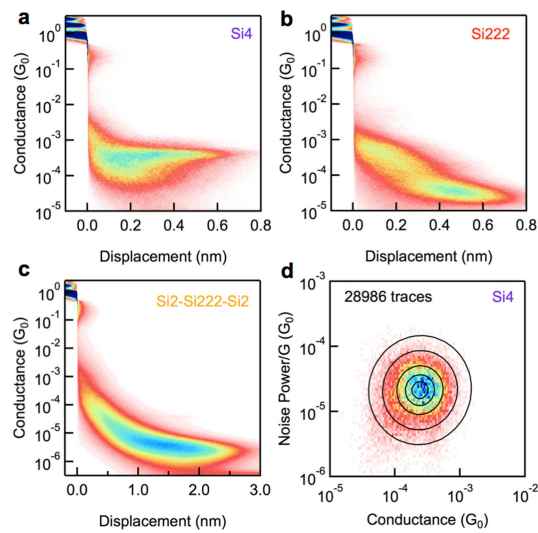
the Fermi energy is observed. This coexistence implies that through-space injection can change the slope of the transmission (and thus the thermopower), without a substantial change in the magnitude of the conductance. Si2-Si222-Si2 at -0.6 eV and Si222 at -1.6 eV both show reversed ring current direction in comparison with that calculated at 0 eV, a clear signature of destructive quantum interference.



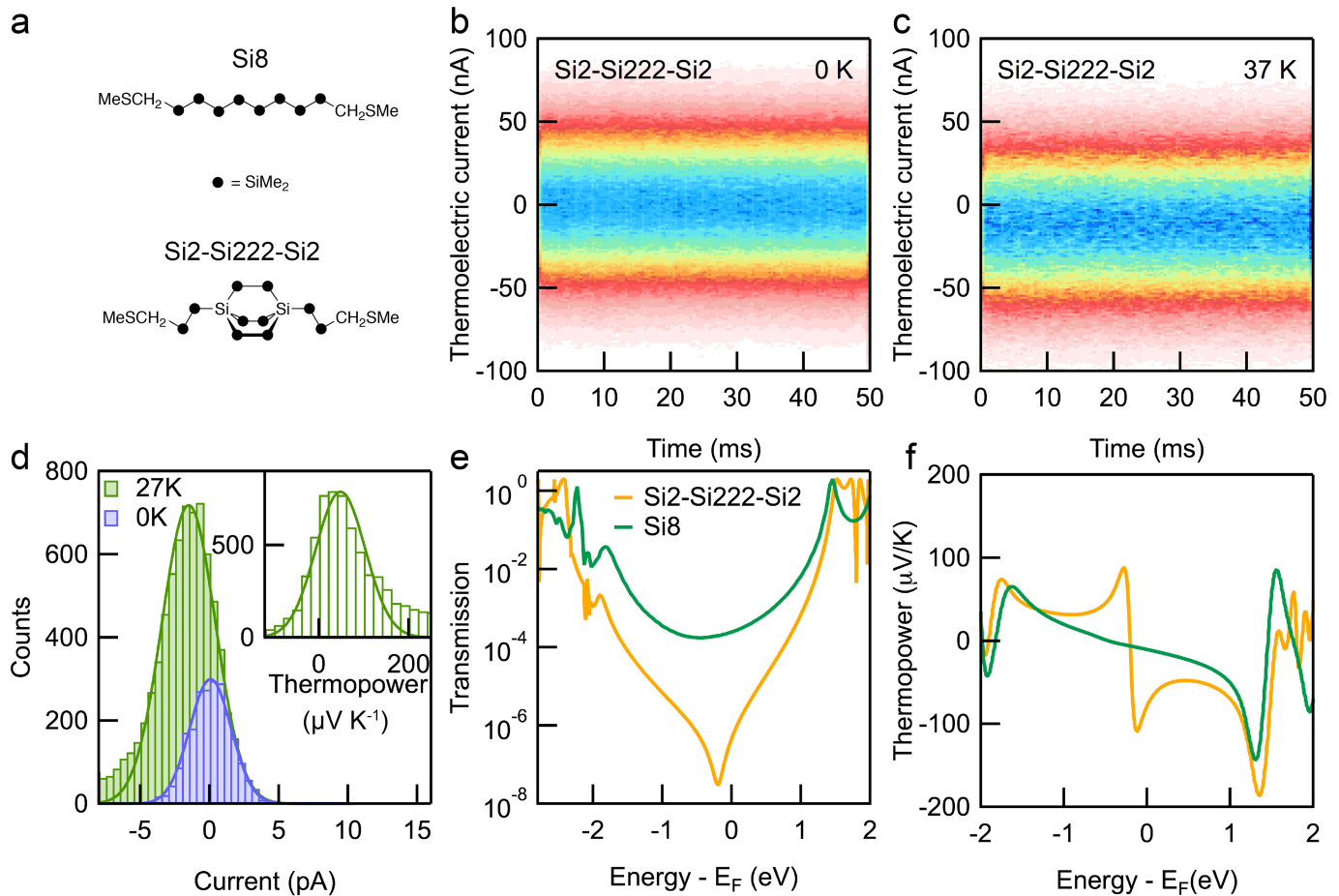
Extended Data Fig. 3 | Transmission of the partially cut versions of Si222. **a**, Chemical structures of Si222-1bridge and Si222-2bridge. **b**, Transmission data of Si222 in anti-conformation with different number of bridges being cut. **c–e**, Transmission pathways are shown for (c) Si222-1bridge (one bridge remains, two were cut), (d) Si222-2bridge (two bridges remain, one was cut) and (e) Si222. The transmission of the Si222-2bridge junction is almost as high as Si222-cut junction where all three bridges are cut, because the bridge where the interference signature appears is cut (d). If we instead cut the other two bridges simultaneously (c, Si222-1bridge), the ring current pathways and the antiresonance in the transmission persist.



Extended Data Fig. 4 | Transmission of linear tetrasilane (Si4) with one bridging unit cut. **a**, Transmission plot of Si4 and Si4-cut, where one $\text{Si}(\text{CH}_3)_2$ unit has been cut away and the bridgehead silicon atoms passivated with hydrogen atoms. **b, c**, Transmission pathways are shown for **(b)** Si4 and **(c)** Si4-cut. **d**, Transmission at the Fermi energy plotted against bridgehead silicon distance of Si4 and Si4-cut. Solid red line is a linear fit to the data of Si4-cut.

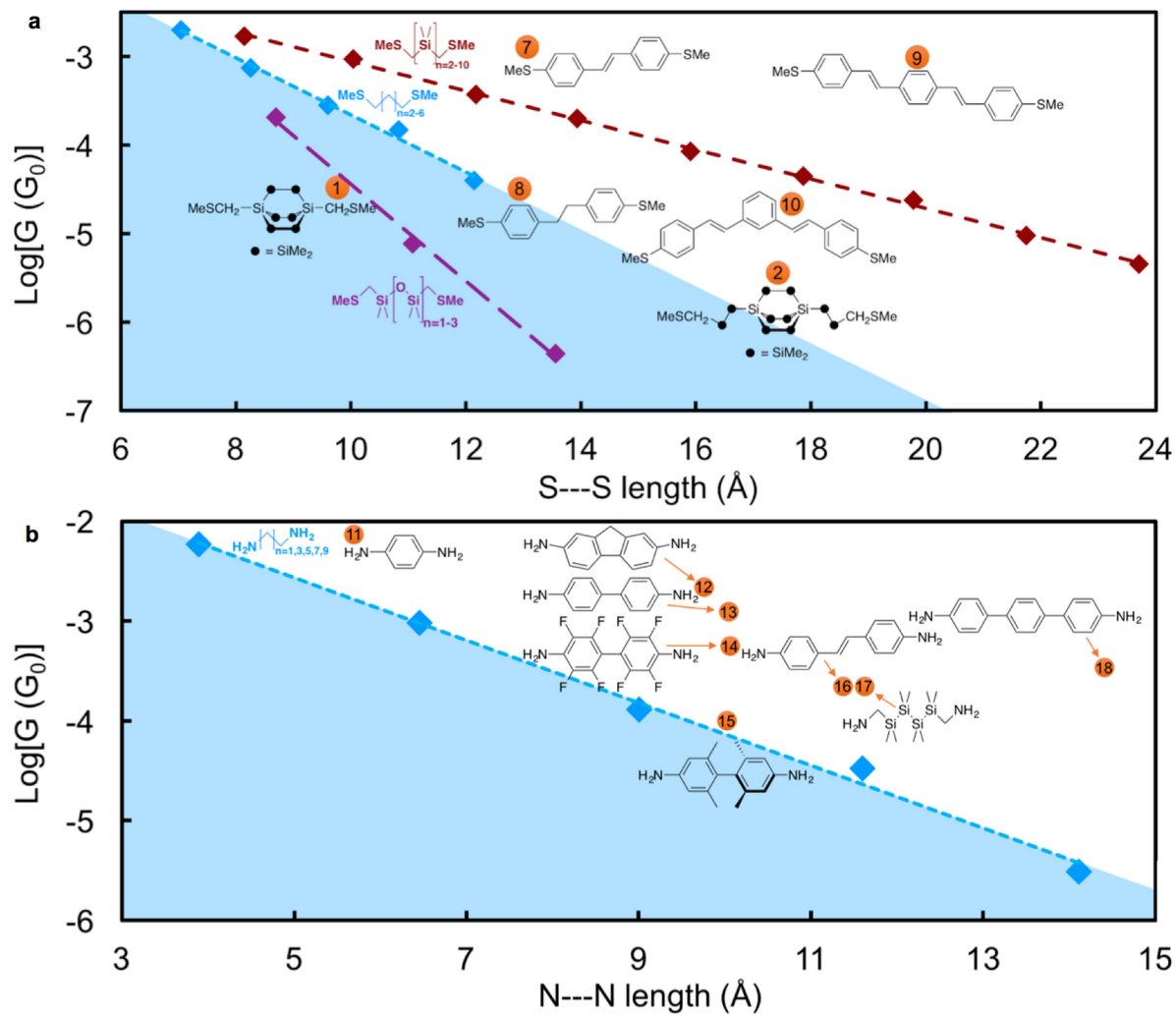


Extended Data Fig. 5 | Experimental 2D conductance versus displacement histograms. **a**, Si4; **b**, Si222; **c**, Si2-Si222-Si2. **d**, Two-dimensional histogram of normalized flicker noise power against average junction conductance for Si4 along with a 2D Gaussian fit of the data. We see almost no correlation between flicker noise power and the conductance and the noise power scales as $G^{1.1}$.



Extended Data Fig. 6 | Thermopower data of Si2-Si222-Si2 and Si8.
a, Chemical structures of **Si8** and **Si2-Si222-Si2**. **b, c**, Two-dimensional histograms of thermoelectric current measured while **Si2-Si222-Si2** junctions are held at $\Delta T = 0$ K and 37 K, respectively. **d**, Histogram of the measured thermoelectric current for **Si8**, which has the same number of Si atoms across the molecule as **Si2-Si222-Si2**, with $\Delta T = 0$ K and 27 K. Inset: Histogram of thermopower determined from the thermoelectric current for **Si8** junctions. After subtracting the thermopower of Au of $2 \mu\text{V K}^{-1}$ (to account for the thermoelectric current between the hot substrate and the

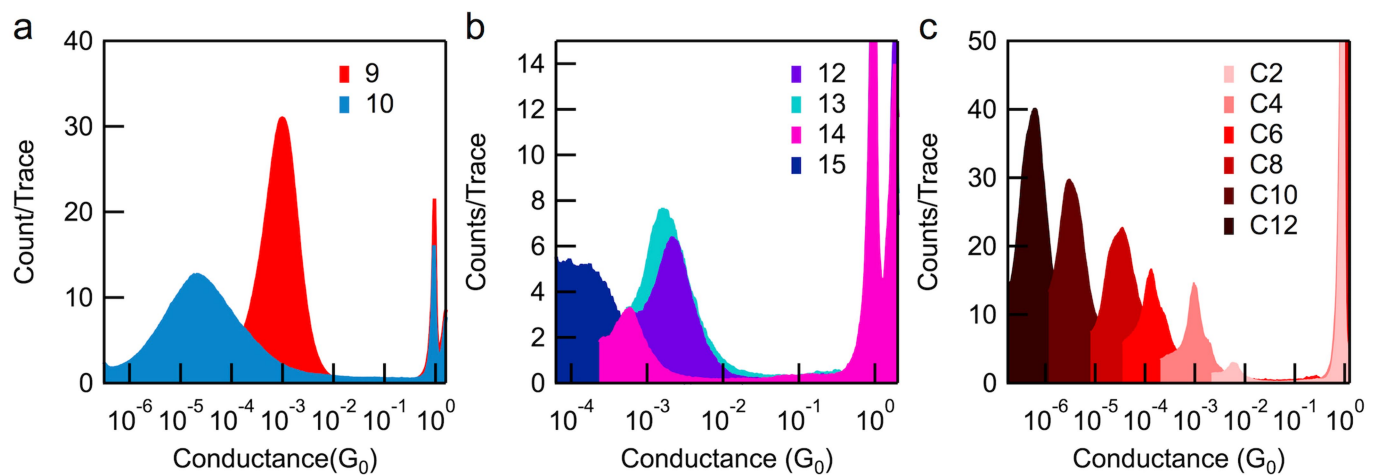
cold set-up), the average thermopower for **Si8** is $35 \pm 17 \mu\text{V K}^{-1}$, smaller than that of **Si2-Si222-Si2**. **e**, Transmission curves for **Si8** junction along with **Si2-Si222-Si2** junction showing different slopes at the Fermi level. **f**, Thermopower calculated as the slope of the transmission as a function of energy. Theory underestimates the thermopower of both **Si2-Si222-Si2** and **Si8** by approximately an order of magnitude. Furthermore, the energy alignment between the antiresonance and the Fermi energy is not exact because of inherent errors of DFT^{31,42}, which results in the opposite sign of the thermopower at the Fermi energy compared to the experimental value.



Extended Data Fig. 7 | Further comparison of experimental conductance of thiomethyl- and amine-terminated molecules.

a, b, Experimental conductance is plotted against calculated (a) sulfur–sulfur distance for thiomethyl-linked molecules and (b) nitrogen–nitrogen

distance for amine linked molecules; dashed lines are linear fits to the data. All conductance values are determined from log-binned conductance histograms created from data taken from references and reproduced in Extended Data Fig. 8^{14,33,43–48}.



Extended Data Fig. 8 | Logarithmically binned 1D conductance histograms for control molecules. a, Molecules 9 and 10; b, molecules 12 to 15; c, amine-terminated alkanes C2 to C12.